Research Square

Preprints are preliminary reports that have not undergone peer review.
They should not be considered conclusive, used to inform clinical practice,
or referenced by the media as validated information.

Landmark-Centered Coding in Frontal Cortex Visual Responses

Adrian Schütz
Philipps University Marburg
Vishal Bharmaurisa
York University
Xiaogang Yan
York University
Hongying Wang
York University
Frank Bremmer
Philipps-Universität Marburg https://orcid.org/0000-0003-1597-7407
Doug Crawford (jdc@yorku.ca)
York University

Article

Keywords: Visual landmarks, spatial cognition, frontal cortex

Posted Date: April 19th, 2021

DOI: https://doi.org/10.21203/rs.3.rs-406838/v1

License: This work is licensed under a Creative Commons Attribution 4.0 International License.
Read Full License

Landmark-Centered Coding in Frontal Cortex Visual Responses

Adrian Schütz[1,2,3]*, Vishal Bharmauria[3,4]*, Xiaogang Yan[4], Hongying Wang[4**], Frank Bremmer[1,2,3], J. Douglas Crawford[3-5**]

* These authors contributed equally
**These authors jointly supervised this work

1. Department of Neurophysics, Phillips Universität Marburg
2. Center for Mind, Brain and Behavior – CMBB, Philipps-Universität Marburg and Justus-Liebig-Universität Giessen
3. Brain in Action International Research Training Program
4. York Centre for Vision Research and Vision: Science to Applications Program
5. Departments of Psychology, Biology, Kinesiology & Health Sciences, York University

Corresponding author:
Dr. John Douglas Crawford
Departments of Psychology, Biology and Kinesiology & Health Sciences
York University, Toronto, Canada
Centre for Vision Research, Room 0009A LAS
4700 Keele Street, Toronto, Ontario, M3J 1P3
Email: jdc@yorku.ca
Phone: 416-736-2100 x 88621
Fax: 416-736-5857

Number of Pages: 38
Number of Figures: 5
Number of supplementary figures: 4
Number of Words (Summary): 150
Number of Words (Introduction/Results/Discussion/Methods): 6329

Running title: Landmark-centered coding in frontal cortex

Conflict of Interest: The authors declare no conflicts of interest

Acknowledgement: This project was supported by a Canadian Institutes for Health Research (CIHR) Grant and the Vision: Science to Applications (VISTA) Program, which is supported in part by the Canada first Research Excellence Fund, and by Deutsche Forschungsgemeinschaft (DFG: IRTG-1901, RU-1847, and CRC/TRR-135, project number 222641018). VB, XY, and HW were supported by CIHR and VISTA. AS was by DFG. JDC is supported by the Canada Research Chair Program.

Abstract

Visual landmarks influence spatial cognition, navigation and goal-directed behavior, but their influence on visual coding for action is poorly understood. Here, we tested landmark influence on prefrontal visual responses by recording from 568 neurons in the frontal (FEF) and supplementary (SEF) eye fields of rhesus macaques. The response field (the area of visual space that modulates activity) for each neuron was tested in the presence of a landmark placed at one of four configurations. We then fit the spatially tuned response fields against a spatial coordinate continuum between gaze- and landmark-centered models. When response fields were fit separately for each target-landmark configuration, the best fits shifted (mean 37% / 40%) toward landmark-centered coding in FEF / SEF respectively, confirming a configuration-dependent intermediate coding scheme. Overall, these data show that external landmarks influence prefrontal visual responses, possibly helping to stabilize movement goals in the presence of noisy internal egocentric signals.

Introduction:

In daily life, we implicitly or explicitly use visual landmarks for navigation and goal-directed behavior [1–3]. For goal directed movement, the initial sensory and final motor systems are fixed relative to the body (i.e., in egocentric coordinates), but intermediate 'representations' are supplemented by world-fixed (allocentric) information, i.e. landmarks [4]. For example, to generate a reach command for a coffee mug on a table, the brain might initially code the location of the mug relative to the eye, but other cues such as edges of the table or a nearby book may modulate these codes before they are converted into shoulder-centered reach commands [5]. To date such influences have been observed in

the brain's memory and motor codes [6–8] but it is unclear how these signals are multiplexed in the sensory inputs to these systems.

Various high-level theories have been postulated for the integration of landmarks with the egocentric codes for action [2,5,9–12]. It has been speculated that the visual system codes this influence as target-landmark configurations [2,13], but the neural mechanisms for this are unknown. Human studies have suggested that egocentric and allocentric visual codes are separated in the dorsal and ventral visual streams, respectively [14–16] and then converge in the frontal cortex for action [8], but again, the mechanisms are unknown.

At the level of cellular physiology, visual receptive fields (the area of space where stimuli influence neural activity) are modulated by the presence of other stimuli within or outside of a response field [17,18]. In particular, it has been reported that landmarks influence neural activity in the superior colliculus [19], parietal cortex [20,21], and precuneus [22]. However, these studies tested the relative influence on response field activity, rather than the underlying coordinate frames used to code this activity.

In a recent series of studies, we used a model fitting approach and a shifting landmark paradigm (**Supplementary Fig. 1**) to test the potential influence of (shifted) landmarks on egocentric and/or allocentric coding in the frontal eye fields and supplementary eye fields (Bharmauria et al. 2020; 2021). We found that, despite the presence of a landmark, neural activity continued to be dominated by eye-centered coding schemes. We further found that a landmark shift influenced target coding in memory and motor responses within this frame. In contrast, we failed to find any influence of a stable landmark on the initial visual response to a transiently presented saccade target. Thus, it remains unclear

how landmark-centred visual information is relayed to frontal cortex, especially in the ecologically normal situation where landmarks remain stable.

Here, we reexamined this question, focusing only on the initial visual response to a target presented briefly in the presence of a stable background landmark **(Fig. 1a).** This time, we tested the hypothesis that visual landmarks influence the prefrontal target response, but in a configuration-dependent pattern. To do this, we employed a similar model-fitting approach as used previously [7,23–26] to determine the coordinates of neural response fields. First, instead of pooling data across different landmark configurations, we separately analyzed different relative target-landmark combinations. Second, instead of testing between sets of idealized egocentric or allocentric models existing in one reference frame each, we developed an algorithm (based on response field weight modulation) to test intermediate egocentric-allocentric models spanning two coordinate systems. Specifically, we tested frames between target relative to fixation (TF) and target relative to landmark (TL) coordinates. This confirmed that prefrontal visual responses are influenced by visual landmarks in a configuration-dependent manner, such that target locations were coded along with a coordinate system that was intermediate between TF and TL coordinates.

Results:

In this study, we investigated the influence of a static landmark on visual responses in two cortical gaze control areas, the FEF and SEF. **Figure 1** shows the visual stimuli that were present before and during the neural responses analyzed in the current study. **Supplementary Figure 1** shows the entire paradigm, including later response periods

that we described in previous studies [6,7,27]. **Figure. 1a** shows an example stimulus configuration where a background landmark (L: a large 'cross') first appears, followed by the target's transient (100 ms) appearance. This cross could appear in one of four spatial (oblique positions) configurations (L1-4) relative to the target stimulus **(Fig. 1b)**. Later, after a delay, monkeys were rewarded for looking at the target stimulus, regardless of any landmark influence **(Supplementary Fig. 1).** Importantly, animals viewed these stimuli head-unrestrained to capture the natural complexity of normal gaze behavior. This includes variable torsion of the eyes around the line of sight, which tends to dissociate retina- and world-fixed geometry. This is a challenge for the visual system [28,29], but useful for dissociating these frames experimentally **(Supplementary Fig. 2).** To account for this, 3D eye orientation was recorded [30], i.e., to precisely calculate the retinal projections of the Target (T) either relative to initial gaze Fixation (TF) or to the Landmark (TL).

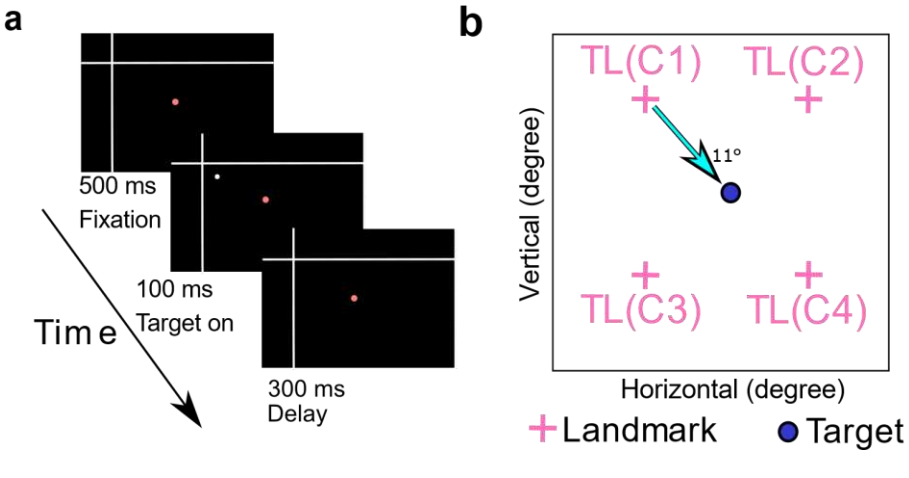

Figure 1: *Experimental Paradigm* ***(a)*** *Initial stages of the memory-delay / landmark paradigm and its time course. The head unrestrained monkey starts the trial by fixating a central red dot for 500 ms in the presence of two white intersecting lines (landmark). Then a white dot (target) is flashed (100 ms) in one of four possible locations relative to the landmark, followed by a 300 ms delay. The remaining parts of the paradigm (not analyzed here) are presented in* ***Supplementary Fig 1. (b)*** *Schematic of the four possible target-landmark configurations (TLC1-4).*

During neural recordings, targets were presented randomly throughout each neuron's response field, while randomly varying the relative landmark configuration, providing a complete dataset for 312 frontal eye field (FEF) and 256 supplementary eye field (SEF) neurons **(Fig. 2a).** Here, we analyzed the response fields corresponding to the initial visual response to the target, quantified as the number of action potentials within a fixed temporal window after target presentation **(Fig. 2 b).**

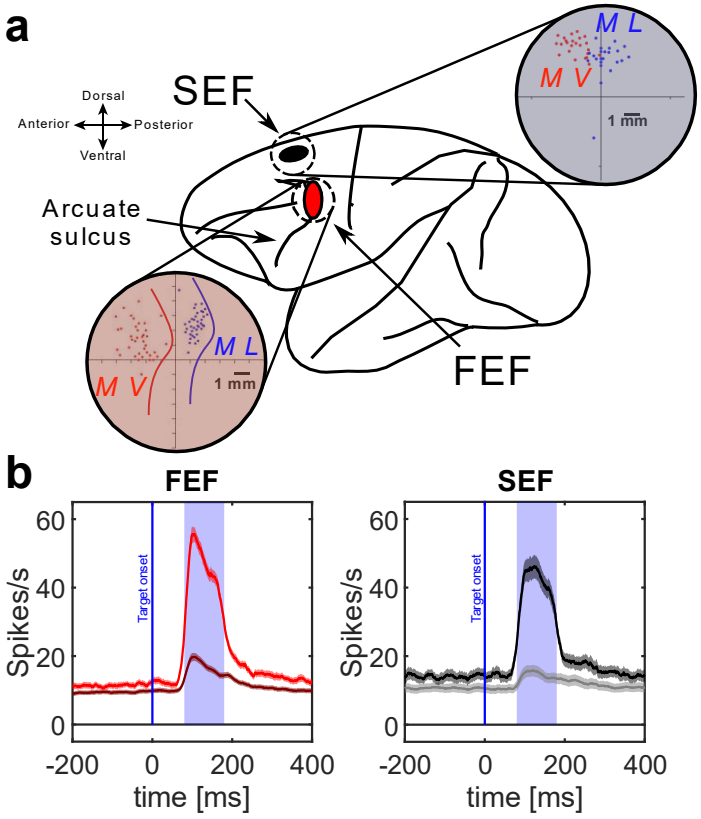

Figure 2: *Electrophysiological recordings* ***(a)*** *The red ellipse represents the location of the FEF, the black ellipse represents the location of the SEF. The connected red and black disks represent the coordinates of our recording chambers, showing the sites (colored dots) of neural recordings for both monkeys (blue Monkey L, red Monkey V), also confirmed by microstimulation-evoked eye movements. Colored lines indicate the location of the arcuate sulcus within the recording chamber for both monkeys* ***(b)*** *Mean (± SD) of the spike-density plots of the visual responses for all FEF neurons (red) and SEF neurons (black/grey) analyzed in this study). The more robust plots (bright red/black) were derived from the top 10% responses for each neuron (corresponding to the 'hot' spot of the neuron's response field used to plot activity in most oculomotor studies), whereas the dark red / gray plots correspond to data from the entire sample (including the top 10%). The shaded areas show the temporal windows used for sampling data to quantify the visual response (ranging from 80ms to 180ms after target onset).*

Finally, using our standard methodology [7,24–26] we fit various models against these spatially tuned response fields, focusing on the intermediate reference frames between TF and TL **(Fig. 3a).** In brief, this involved performing non-parametric fits to the visual response as a function of two-dimensional target location, defined in a specific spatial reference frame **(Fig. 3b)**. The spatial reference frame that yielded the lowest residuals (between the fit and the actual data) was deemed to be the best 'model'. This is essentially the same principle used in classic reference frame studies [31,32] but generalized and quantified to allow fits to any spatial model in the presence of variable and arbitrary behavior. To test the intermediate reference frame hypothesis, we weighted the two models against each other, thus generating a mathematical continuum between TF and TL **(Fig. 3c1**), yielding response field fits for each of these points [24], where again the fit with lowest residuals 'wins' **(Fig. 3c2).**

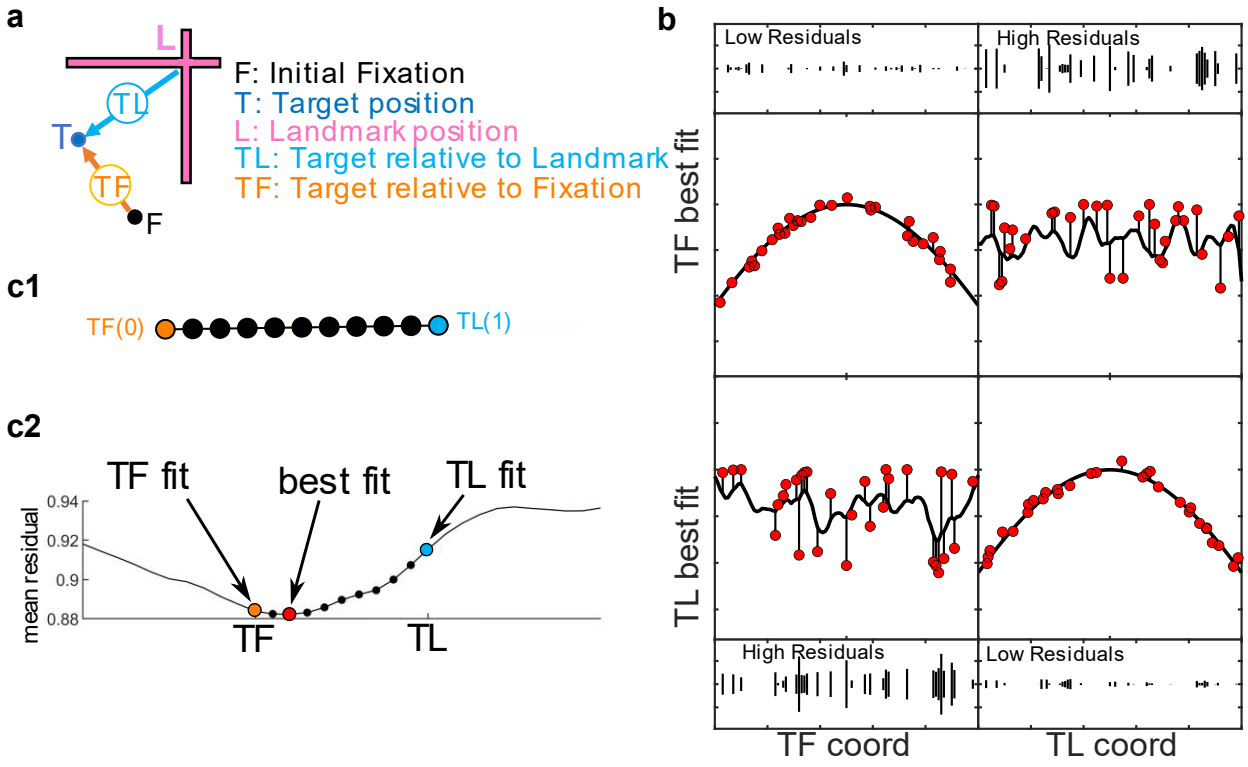

Figure 3: (a) *Schematic for the spatial parameters of a single trial. The target position (TF) is shown in dark blue, the landmark position (L) is shown in magenta, the target position relative to the landmark (TL) is indicated by a cyan arrow, the initial fixation is indicated by the black dot and the target relative to initial gaze fixation (TF) is shown as an orange arrow. All positions were calculated in eye coordinates* ***(b****) Schematic of the logic behind the response field analysis. The x-axes represent the spatial coordinate. The y-axes show neural activity. Neural responses from individual trials are represented by the red dots. The black curving lines show the non-parametric fits which do not restrain the response field to a specific (e.g. gaussian) shape. The upper-left square shows activity from a neuronal response field that is tuned to TF coordinates and plotted relative to TL coordinates, resulting in a good fit with low residuals (difference between the fit and data, shown as vertical lines). The upper-right square shows activity from a neuronal response field tuned to TF coordinates but plotted in TL coordinates, resulting in a poor fit. Conversely, TF coordinates will provide poor fit, and TL coordinates will provide a good fit to a neuron tuned to TL coordinates (bottom panels).* ***(c):*** *Fitting data to intermediate TL-TF coordinates.* ***(c1)*** *Black circles show intermediate steps along the mathematical continuum between TF (represented as 0) and TL (represented at 1.0) Exemplary TF (orange) to TL (cyan). The red spot represents the best fit in the following example.* ***(c2)*** *Lower row: mean residuals for fits along the TF-TL continuum, including purely TF (orange), optimal (red), and TL (cyan) fits.*

In a preliminary step for analysis, we determined that 102 of our FEF and 43 of the SEF recorded neurons showed statistically significant spatial tuning for the target in their visual response fields (see methods), and thus (only) these qualified for our model-fitting procedures. In our previous studies, we compared fits for an exhaustive set of egocentric and allocentric models and found that FEF and SEF visual responses showed a significant preference for target position in eye coordinates when the data were pooled across different T-L configurations [6,7]. Technically, these coordinates were computed by rotating the eye-target vector by the inverse of initial 3D eye orientation, but we will refer to this as target-relative to fixation (TF) for simplicity.

Figure 4 provides an example of the visual response from one such FEF neuron. **Figure 4a** represents the raster and spike density plot for all and the top 10% (red) of neural responses. The top 10 % roughly correspond to the 'hot spot' of the response field as typically used. The blue shaded area (80-180 ms aligned to target onset) corresponds to the temporal sampling window used for the response field plots/fits. **Figure 4b** shows the response field of the neuron, here including all trials, plotted in TF coordinates. Note that here, we pooled across results for all four target-landmark configurations, as indicated by the insets. The black circles superimposed on the colormap denote the stimulus location and their diameter the the number of action potentials in the visual response window for a given trial, whereas the color of the underlying colormap indicates the non-parametric fits to the pooled response field. **Supplementary Figure 3b** shows an SEF example, plotted the same way. Note that there is some variability in visual target response (circle) size for any one point on the response field map. This occurs when the ideal coordinate frame is not used for the plot **(Fig. 3b),** but even for the best model, some variability (residuals) persists due to non-spatial factors such as attention and motivation [6,7,33,34].

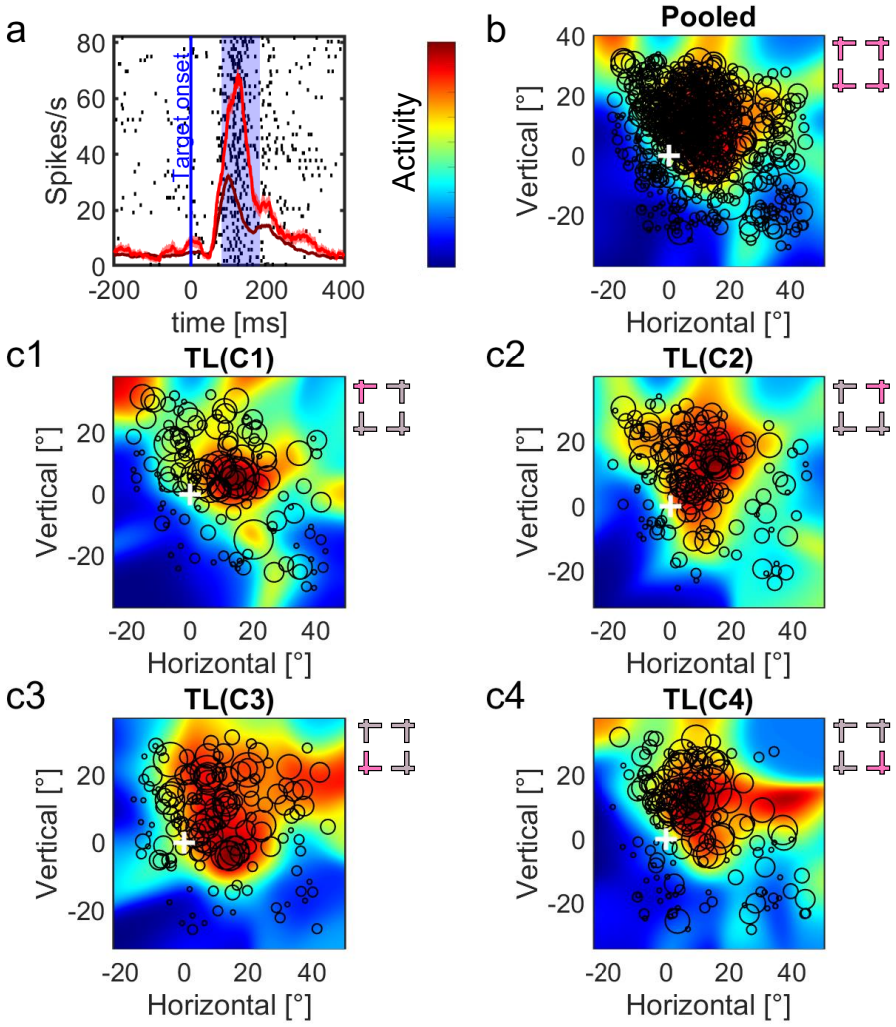

Figure 4: *Typical example of a visual response field analysis (in this case for an FEF neuron).* ***(a)*** *Raster and spike density plot of the neuron's activity. The blue vertical line indicates the target onset and the blue shaded area the time window (80ms to 180 ms after target onset) used to quantify the visual response to the target. The dark red line shows the spike density for all trials (including the top 10%), the bright red line the activity for the 10 % trials with the highest activity in the analysis window. The confidence intervals show the standard error.* ***(b)*** *Shows the non-parametric fit of the neuron's response field, pooling data across all four landmark configurations (indicated by magenta crosses). The color scale on the left indicates the fit to activation ranging from low (blue) to high (red). The black circles indicate responses from individual trials, placed at the target stimulus's location and the diameter scaled to the response in the sampling window. The white crosses indicate the 0,0 point (fovea) in this coordinate system.* ***(c1-c4)*** *Shows a similar analysis but computed separately for each landmark configuration (TLC1-4, indicated in magenta).*

For the first step in our new analysis, we separated and plotted the response fields for each of the four target-landmark configurations (**Fig. 4 c1-4**, where the landmark configuration is highlighted in each of the corresponding insets). This still resulted in good fits, i.e., with similar degrees of significant spatial tuning. Typically, the four TLC fits showed similar response field shapes and 'hot spot's, differing only in small, variable shifts and distortions (most likely resulting from idiosynchratic sampling biases that have little to do with the underlying coordinate systems). The same occurred when we separated the SEF data by target-landmark configuration **(Supplementary Fig.3 c1-4).**

To test the influence of these different landmark configurations on the target response coordinates, we developed and tested various egocentric-allocentric continua, finding the TF-TL (Target-relative to landmark). Since these calculations were based on a non-parametric fitting procedure, they are relatively immune to the small response field idiosyncrasies noted above [24]. We then applied this analysis both to the pooled dataset (as a control) and the configuration-dependent dataset across the entire populations of spatially tuned neurons in the FEF neurons (N = 102) and the SEF (N = 43) to find optimal fits along the TF-TL continuum. We found no significant difference (Friedman's ANOVA, FEF: $p = 0.59$ SEF: $p = 0.46$) between the distribution of preferred coding along the TF-TL continuum *between* the four different target-landmark configurations in either the FEF or SEF **(Supplementary Fig. 4)**. Therefore, to obtain one representative fit for each neuron, we recombined the configuration-specific fits by averaging the amounts of TF-TL shift across the four (TLC 1-4) configuration fits for each neuron, thereby normalizing their directional influence.

Figure 5 contrasts the population distributions of the pooled (*left*) and direction-dependent / recombined fits (*right*) along the TF(0)-TL(1) continuum for both the FEF (**a**) and SEF (**b**). These distributions are illustrated as 'violin plots', which provide more information than standard mean ± variance of box plots. For the FEF (**Fig. 5a**) the distribution of fits for the pooled analysis peaked near the TF frame (mean = 0.17 median = 0) with no significant influence of the landmark ($p = 0.13$, one sampled sign test), suggesting either that the visual response only codes Target-relative-to-Fixation (TF), or that the landmark influence is obscured when different target-landmark configurations are pooled. Consistent with the latter possibility, the distribution for the configuration-dependent / recombined dataset (right) showed a significant shift toward the TL frame (mean = 0.45, median = 0.5, $p = 3.39*10^{-19}$ one sampled sign test), suggesting an influence of landmark on the visual responses of FEF neurons. This was also the case for the uncombined target-landmark configurations **(Supplementary Fig. 4a).** There was also a significant difference between the direction-dependent data and the pooled control data (two sampled sign test, $p = 4.39*10^{-12}$), showing that the landmark influence was configuration-dependent.

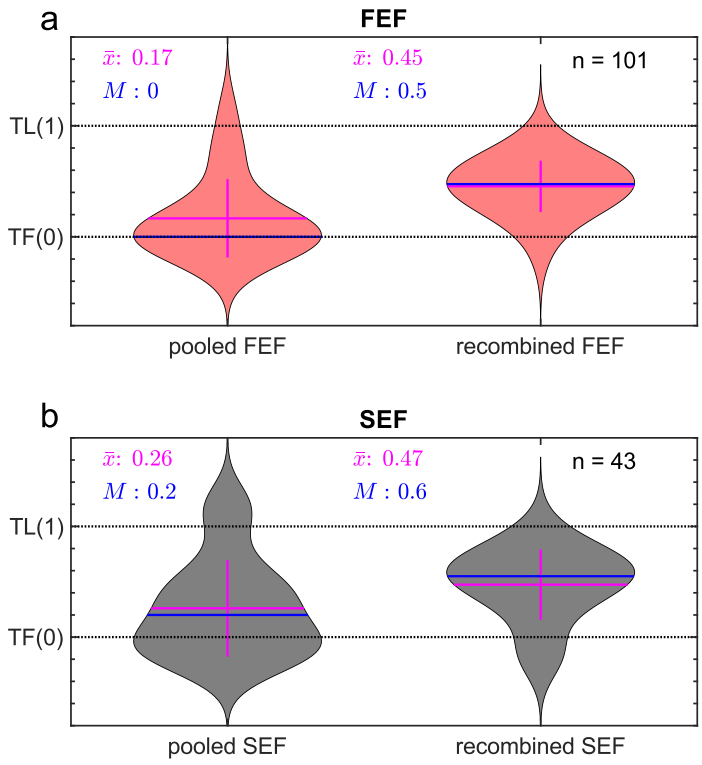

Figure 5: *Violin plots of the distributions of best fits along the TF-TL continuum for all spatially tuned FEF neurons* ***(a)*** *and SEF neurons* ***(b).*** *The left side plots show fits made to the pooled data (across all four landmarks) for each neuron; the right-side plots show fits derived separately for each landmark configuration, then recombined by averaging the TF-TL score for each neuron. Blue lines represent the median; magenta lines represent the mean. FEF neurons (a) showed no significant deviation from TF(0) (mean = 0.17, median = 0) in the pooled analysis whereas the separate / recombined distributions (mean = 0.45, median 0.5) were significantly shifted toward TL(1). Likewise, SEF neurons (b) showed no significant shift from TF (mean = 0.26, median = 0.2), whereas the separate / recombined distributions (mean = 0.47, median = 0.6) were significantly shifted toward TL. See text for statistical details.*

Figure 5b provides a similar analysis for the SEF (n = 43). Overall, we observed the same trends in the SEF as for the FEF. We found no significant shift toward TL (mean = 0.26, median = 0.2, p = 0.06, one sampled sign test) in the pooled analysis (left), i.e., the visual response was best described by the TF model. For the configuration-dependent / recombined analysis (right), we found a significant shift (mean = 0.47, median 0.6, p = $4.43*10^{-7}$, one sampled sign test). Again, this effect was also evident when landmark configurations were tested separately **(Supplementary Fig 4b)**. Furthermore, there was

a significant difference between the pooled data and the direction-dependent data (two sample sign test, $p = 2.94*10^{-4}$) indicating a configuration-dependent landmark influence.

Finally, to test these results and the single cell level and ensure that they were not an artifact (i.e., of some interaction between our fitting method and the separate configuration analysis), we tested the result of every individual neuron, and every configuration relative to a randomized baseline (ranksum test). The randomized baseline was created by a reiterative 'shuffling' process described in the methods. In this case we also included neurons without spatial tuning as an additional control. This showed that most neurons in both the FEF and the SEF display a significantly shifted coding behavior (**Fig. 6**, yellow cells) relative to the randomized baseline. All spatially tuned neurons showed a a significant shifted coding for at least one TLC. In contrast, neurons that did not show significant tuning for any TLC did *not* show a significant landmark influence. Since this test showed a landmark influence relative to randomized data, and only for spatially tuned neurons, our landmark effect did not result from a methodological artifact. Overall, this test confirms that the population landmark influence (**Fig. 5**) is present at the single neuron level (**Fig. 6**), is a specific property of spatially tuned neurons.

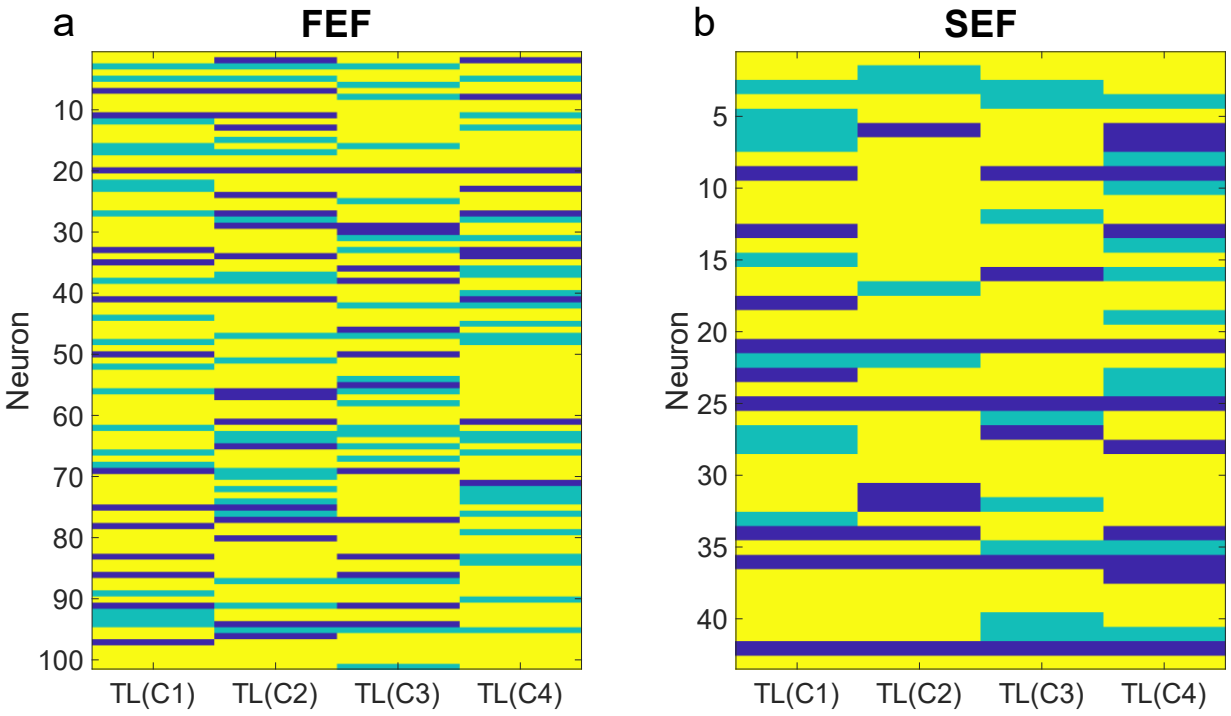

Figure 6: Neuron-by-neuron significance test for TF-TL shift, broken down by Landmark configuration (TLC 1-4). Left: FEF neurons Rigt: SEF neurons. The y axis identifies the neuron, the x axis the represents the TLC. Yellow cells are significantly different. From their respective randomized baseline describes in methods. Cyan cells are not significantly different. Blue cells are untuned neurons.

Discussion

In summary, our analysis shows that visual landmarks can influence the visual code in both the FEF and the SEF. More specifically, the landmarks caused a shift in the reference frame for coding the target toward the landmark (TL), and further, this influence was dependent on specific target-landmark configurations. This is not the first time that the frontal cortex has been implicated in allocentric coding. For example, it has been implicated in object-centered coding (one part of an object relative to another) [35,36], and our studies have shown that prefrontal memory and motor responses are involved in integrating conflicting ego/allocentric cues [6,7]. However, to our knowledge, this is the first study that has shown the influence of a stationary, independent and behaviorally irrelevant landmark on frontal cortex visual signals to a potential movement target.

It is important to note that this TF-TL shift does not mean response fields shifted toward the landmark, which might indicate a simple shift in the perceived target direction. The small response field shifts that we observed (e.g., **Figure 4 c3)** were highly varable and did not follow any clear pattern across neurons. Instead, we are talking here about a more fundamental shift in the underlying coordinate frame used to encode these responses. Specifically, the neuron's response was dictated by both the location of the target relative to the initial gaze fixation point (TF) *and* the landmark (TL). Based on our response field fitting method, that optimal point was intermediate, shifted away from TF toward TL.

Further, when we pooled data across all TL configurations, their influence was no longer evident, suggesting that the landmark's neural influence depends on its direction relative to the target (or vice versa: TL). In other words, the visual system seems to implement

this influence through forming specific landmark-target linkages rather than a global algorithm that works across configurations. These are likely the reasons why our previous studies failed to find a landmark influence in frontal visual responses [6,7].

One difference from our experimental paradigm and the natural world is that the latter is generally replete with potential landmarks. It is possible that the observable influence of these landmarks would usually cancel (like in our pooled data), but this does not mean they would have less influence on behavior. Indeed, an extensive background shift has more influence on visual responses than a slight landmark shift [22], and conversely, should have a more stabilizing influence on vision and behavior when stationary. Further, in real-world conditions, not all landmarks are equal: landmarks differentially influence behavior based on salience, distance, reliability, and prior experience [3,9,10,37,38]. Thus, our landmark task approximates the case where the visual response is dominated by a single nearby, salient, and stable landmark.

The finding that frontal cortex visual responses utilize an intermediate TF-TL code suggests that the visual system is directly involved in integrating egocentric (e.g., eye centered) and allocentric (e.g., landmark-centered) cues, but where and why does this occur? One possibility is that the landmark-centered coding described here helps to compensate for variations of the initial eye and head orientation, including eye torsion in space, which is quite large and variable in head unrestrained conditions **(Supplementary Figure 2 a)** and likely helped to distinguish the TF and TL models **(Supplementary Figure 2 c).** It is thought that internal copies of the eye and head orientation are used to

compensate for these effects [29,39], but visual landmarks can help stabilize noise in these signals [9,27]. The recent finding that some occipital neurons compensate for eye torsion suggests that the early visual cortex might already contribute to this function [40].

How could such visual responses influence the frontal cortex? Occipital cortex projects both to the parietal cortex, mainly associated with egocentric coding, and the temporal cortex, which is associated with allocentric coding [2,8,15]. However, there is considerable cross-talk between the ventral and dorsal stream [41–43]. The parietal cortex also shows landmark influence in some visual and memory-guided saccade tasks [13,22] and projects to both the SEF and the FEF [33,44]. It is likely that these pathways are responsible for the allocentric influence in the visual signals observed in the current study and that these visual signals, in turn, are responsible for the influence of a landmark shift on FEF/SEF memory and motor responses that we observed in our previous studies [6,7].

To our knowledge, there is no precedent for this type of coding in visual responses within the motor system, but how does this map on to other systems? Place cells and grid cells in the hippocampus account for visual landmarks in the processing of relative location for memory and navigation [45,46]. However, recent evidence implies that the hippocampus may derive these signals from as early as the primary and extrastriate visual cortex for the coherent encoding of the spatial behavior [47–50]. Given that the visual system is connected to the frontal areas [51–53], altogether, the factors suggest that the visual system itself may play a more sophisticated role in preprocessing allocentric and egocentric cues for other systems, including the sensorimotor system, than previously suspected.

Methods

Experimental details have been published previously [6,7] but are summarized here, along with descriptions of the new configuration-dependent and intermediate ego-allocentric frame analysis methods employed here.

Surgical Procedures and recordings of 3D Gaze, Eye and Head

All experimental procedures were approved by the York University Animal Care Committee and were in accordance with the guidelines of the Canadian Council on Animal Care on the use of laboratory animals. The neural data used in this study were collected from two female *Macaca mulatta* monkeys (Monkey V and Monkey L). Both animals were implanted with 2D and 3D search coils. Both search coils had a diameter of 5 mm and were implanted in the sclera of the respective animal's left eye. The recording chambers for both animals were implanted centered at 25 mm anterior and 19 mm lateral for FEF and 25 mm anterior and 0 mm lateral for SEF. Surgeries were performed as done previously [30]. Underneath each chamber was a craniotomy of 19 mm diameter to allow access to the right FEF and right SEF, respectively. During the experiment, the animals were placed in a custom-made primate chair modified to allow free head movements.

Additionally, the monkey was suited with a vest connected to the primate chair to restrict it from rotating around in the chair. Furthermore, two orthogonal coils were mounted on the head of the monkeys during the experiment. The animal was then placed in the setup, which was equipped with three orthogonal magnetic fields. These fields induced a current in each coil. The amount of current induced by one of the fields is proportional to the coil area parallel to this field. Thus, allowing to derive the orientation of each coil in relation to

the magnetic fields and in turn, the orientations, velocities and accelerations of the eye and the head of the animal [30].

Behavioral Paradigm

Using a back projector (NEC UM330X), the visual stimuli were presented on a flat screen located 80 cm in front of the animal. The animals were trained on a memory-guided cue-conflict saccade task, where the monkey had to perform a saccade to a remembered target relative to an allocentric landmark (two intersecting lines) that shifted during the memory delay after a mask presentation **(Supplementary Fig. 1).**

Each trial started with the monkey fixating a red dot located centrally on the screen for 500 ms in the presence of the landmark. Then a white dot serving as visual target was briefly flashed for 100 ms in one of four oblique positions relative to the landmark vertex. Within the context of this paper, each of these target-landmark combinations will be called target landmark configurations [TLC1 (45°), TLC2 (135°), TLC3 (-135°) and TLC4 (-45°)]. For example, TLC1 refers to the Target-landmark configuration where the landmark was present at a 45 ° angle 11° away from the target. Following a delay of 300 ms a grid-like mask was displayed for 200 ms to occlude visual traces of the landmark. After the offset of the mask, the landmark reappeared either shifted (90 %) by 8° in one of eight equally spaced radial directions or not shifted (10%). Following a random delay between 200-600 ms the fixation point disappears acting as a go signal for the animal to initiate a saccade. If the gaze of the monkey landed anywhere in an 8-12° radius around the original target position, the monkey received a droplet of water as reward. This large reward window ensured the monkey was not biased towards either the original target location or the

virtually shifted target location fixed to the shifted landmark. Note that all angles mentioned in this section were assumed to be linear. This means an 8° shift in the center of the screen stretches over the same distance on the screen as an 8° shift at the outskirts of the screen.

Behavioral Recordings, Electrophysiological Recordings, Response Field Mapping and Data Inclusion

During the experiment, three-dimensional eye and head orientations in space were recorded at a sampling rate of 1 kHz using the implanted and head-mounted search coils respectively. These (as well as target and landmark locations) were recorded, analyzed offline and then used as to compute the spatial coordinates for various model fits, such as TF, TL, and various others [6,7].

The neuronal activity **(**Fehler! Verweisquelle konnte nicht gefunden werden.**b)** in the FEF and the SEF was recorded in parallel with tungsten microelectrodes (0.2-2.0 mΩ, FHC Inc.) using the 64 channel Plexon MAP system. To lower the electrodes, the Narishige MO-90 hydraulic micromanipulator was used. The recording sites of the FEF and the SEF were confirmed by using a low-threshold (50 µA) electrical microstimulation while the head was restrained as defined previously [54]. Neurons were mostly searched for while the animal was head-unrestrained scanning its environment. When a reliably spiking neuron was found, the experiment was started. After an initial sampling period for the response field's dimensions, we presented targets (randomly one-by-one) in a 4 x 4 to 7 x 7 array (each 5-10 ° apart from each other) spanning 30-80° across horizontal and

vertical dimensions. We aimed to record approximately 10 trials/target, so the bigger the response field (and thus the more targets), the more the number of recorded trials was required and vice versa.

For analysis of the visual activity, a fixed 100-ms sampling window was chosen, ranging from 80-180 ms after the target's onset. Only neurons that showed significant activation in the sampling window were included in the analysis **(**Fehler! Verweisquelle konnte nicht gefunden werden.**b).** Furthermore, trials in which the animals did not successfully fixate on the home position were excluded.

QUANTIFICATION AND STATISTICAL ANALYSIS

Fitting neuronal response fields against Spatial Models

Using the same spatial model-fitting approach that we have employed in this study, we have shown that SEF and the FEF visual response code for target direction in eye (TF) coordinates [6,7]. To examine the influence of the stable visual landmark on the neural activity, here we specifically explored two spatial models **(Fig. 3a):** 1) the target position in eye coordinates (TF) and 2) the target position in relation to the landmark projected in eye coordinates (TL). The former was computed by rotating each target direction vector by the inverse of 3D eye orientation space at the viewing time [55]. The latter is derived by calculating the vector between the landmark and the target and then projecting this vector onto the retina with respect to the 3D-eye position $Q_F(i)$.

$$TF_i = Q_{F_i}^{-1} T_i \qquad TL_i = Q_{F_i}^{-1}(T_i - L_i) \tag{i}$$

To differentiate between different spatial models, they must be spatially separable [24,26]. This variability is ensured by the stimulus design (e.g., random fixation position) and the animal's natural behavior. Further, opposed to decoding approaches which typically test the set of parameters is implicitly coded in population neuronal activity [56,57], our technique directly tests which underlying spatial model best explains variation in the neuronal activity. The response fields of neurons (A) were fitted against the different spatial models (here TF and TL) using a non-parametric fit with a Gaussian kernel in conjunction with Euclidian distance (d) seen in equation (ii) and (iii).

$$d_{TF,i,j} = \sqrt{\left(TF_i - TF_j\right)^2} \qquad d_{TL,i,j} = \sqrt{\left(TL_i - TL_j\right)^2} \tag{ii}$$

$$A_{fit}(TF_i) = \sum_{j \neq i}^{n} A(TF_j) e^{-\left(\frac{d_{TF,i,j}}{KW}\right)^2} \qquad A_{fit}(TL_i) = \sum_{j \neq i}^{n} A(TL_j) e^{-\left(\frac{d_{TL,i,j}}{KW}\right)^2} \tag{iii}$$

To quantify the quality of the fit (A_{fit}), the predicted residual error sum of squares (PRESS) statistics was used. These residuals were calculated for each trial by fitting the response field by subtracting the data from the left-out trial and then comparing the activity predicted by the fit for the spatial properties present in the trial and the actual activity measured during the trial. Afterward these residuals were squared and averaged across each trial to derive PRESS value for a given fit. The bandwidth of the Gaussian kernel (KW) was determined for each neuron individually to match the response field's size, shape, and contour [24]. This was done by calculating the PRESS statistic for each spatial model for all bandwidths between 1 and 15. Then the bandwidth yielding the lowest residuals was deemed as the best fit or spatial model. A schematic of this is displayed in **Figure 3b-c.**

Put simply, neural data plotted in the correct reference frame/spatial model would lead to least residuals, e.g. a target-fixed response field would fit best in target-fixed coordinates, whereas in an incorrect frame (e.g. shifted toward Landmark), the data would not fit better, yielding higher residuals. In other words, an intermediate TF-TL point yielded the lowest residuals between the fit and the data, thus best explaining variability in the data. In separate TL configurations, the target-landmark vector was fixed, but variations in initial eye orientation cause this to vary relative to the retina, thus separating TF and TL (**Supplementary Figure 3).** This is why our behavioral recordings were important: variations in eye orientationare larger and more variable without head restraint [30], and 3D eye recordings were needed to account for this.

Pooled vs. Separate analysis

Previously, when we only analyzed the visual response we did not find any landmark influence in FEF and SEF [6,7], because we pooled the data across all target landmark configurations and did not consider the TF-TL continuum. Here, to quantify the influence of the landmark we contrasted two analysis conditions (pooled and separate). In the pooled condition (also referring to it as direction-independent), all trials of a given neuron were analyzed together, i.e., the response fields were fit with all the data across all the trials for a given neuron. Thus, resulting in a coding preference independent of the TLC **(Fig. 3c)**. However, this can be argued since it can be assumed that the possible influences of the different landmarks are canceled out if all TLCs are combined due to them being oblique. For the separate condition, trials were grouped with respect to the

specific TLC **(Figure 1b).** i.e., the response fields were fit with the neural data from the trials only corresponding to a landmark in a specific direction (also referred to as direction-dependent analysis). Thus, resulting in four coding preferences/conditions for each neuron (one for each TLC). Since in this pipeline all TLCs are viewed individually, the effects of the landmarks will not cancel out. Note: it is variations in 3D orientation of the eye at fixation that distinguish between the two models **(Supplementary Fig 3).**

Intermediate spatial models

Our previous results [6,7,23,25,26] suggested that neuronal response fields do not always exactly fit canonical spatial models like TF, but instead might best be described by intermediate models between canonical ones **(Fig 3c).** However, in those studies we only looked at intermediate models within or between egocentric frames of reference, using linear interpolation. In this study, we investigated spatial models that exist between egocentric and allocentric frames (iv, v, vi). This makes it impossible to calculate intermediate spatial models by interpolation. So instead, we incorporated a weighting factor (w) into our algorithm (v, vi). We first calculated the distances (d) between trials used in the non-parametric fit used for response field fitting by calculating the Euclidian distance (v) between four-dimensional vectors representing the trials.

$$TF_i = \begin{pmatrix} x_{TF,i} \\ Y_{TF,i} \end{pmatrix} \quad TL_i = \begin{pmatrix} x_{TL,i} \\ Y_{TL,i} \end{pmatrix} \tag{iv}$$

$$d_{w,i,j} = \sqrt{\left(\begin{pmatrix} wTF_i \\ (1-w)TL_i \end{pmatrix} - \begin{pmatrix} wTF_j \\ (1-w)TL_j \end{pmatrix}\right)^2} \quad \text{(v)}$$

$$A_{fit,w}(TF_i, TL_i) = \sum_{j \neq i}^{n} A(TF_j, TL_j) e^{-\left(\frac{d_{w,i,j}}{KW}\right)^2} \quad \text{(vi)}$$

TF gives the first two elements of these four-dimensional vectors, and the last two elements are given by TL. The continuum is derived by weighting the first two elements against the last two elements during the Euclidian distance calculation. Thus, the continuum ranges from TF (weight of TF = 1, weight of TL = 0) to TL (weight of TF = 0, weight of TL = 1) with nine steps in between **(Fig. 3)**. An example of response field fitting for a continuum between two reference frames (TF and TL) is displayed in **Figure 3c2**. Displayed are the residuals for each fit along the continuum ranging from TF(0) to to TL(1) with the best fitting step being 0.2 (red dot).

Test for spatial tuning

The method described above assumes the response fields of the neuron are spatially tuned. This does not imply that the spatially untuned neurons do not contribute to the code [58–61], but with our technique only the spatially tuned neurons can be explicitly tested. To test for spatial tuning the firing rate data was shuffled over the position data obtained from the best-fitting model[24,26]. The mean PRESS residual distribution ($PRESS_{random}$) of

the 100 randomly generated response fields was then statistically compared with the mean PRESS residual ($PRESS_{best\text{-}fit}$) distribution of the best-fit model (unshuffled, original data). If the best-fit mean PRESS fell outside of the 95% confidence interval of the distribution of the shuffled mean PRESS, then the neuron's activity was deemed spatially selective. At the population level, some neurons displayed spatial tuning at certain time-steps and others did not because of low signal/noise ratio. Thus, we removed the time steps where the populational mean spatial coherence (goodness of fit) was statistically indiscriminable from the baseline (before target onset) because there was no task-related information at this time and thus neural activity exhibited no spatial tuning. We defined an index (Coherence Index, CI, vii) for spatial tuning, which was calculated as [62]:

$$CI = 1 - (PRESS_{best\text{-}fit}/PRESS_{random}) \quad \text{(vii)}$$

If the $PRESS_{best\text{-}fit}$ was similar to $PRESS_{random}$ then the CI would be roughly 0, whereas if the best-fit model is a perfect fit (i.e., $PRESS_{best\text{-}fit} = 0$), then the CI would be 1. We only included those neurons in our analysis that showed significant spatial tuning.

Test against randomized baseline

To verify that the coding preference changes in the separated analyses correlated with the TLC we tested each individual neuron's coding for each of the four TLC groupings relative to a randomized baseline. This baseline was constructed by randomly grouping trials for the separate analysis. The randomized groups matched the actual groups (grouped by TLC) in their number of elements. The randomized groups were analyzed in

the same way as the actual groups. This procedure was repeated one hundred times. Thus, resulting in a distribution of coding for each of the four groups. This distribution is subject to the same analysis as the actual groups but due to being randomized, direction-specific influences are averaged out. Thus, this distribution is serving as a baseline for the direction specific influence of the landmark. This means that a significant deviation from the baseline indicates a significant direction-specific influence of the landmark.

Statistical analysis

All statistical analyses were performed using MATLAB R2019b. We assumed a significance level of $p < 0.05$.

REFERENCES

1. Camors, D., Jouffrais, C., Cottereau, B. R. & Durand, J. B. Allocentric coding: Spatial range and combination rules. *Vision Research* **109**, 87–98 (2015).

2. Filimon, F. Are All Spatial Reference Frames Egocentric? Reinterpreting Evidence for Allocentric, Object-Centered, or World-Centered Reference Frames. *Frontiers in human neuroscience* **9**, 648 (2015).

3. Neggers, S. F. W., Schölvinck, M. L. & van der Lubbe, R. H. J. Quantifying the interactions between allo- and egocentric representations of space. *Acta Psychologica* **118**, 25–45 (2005).

4. Crawford, J. D., Henriques, D. Y. P. & Medendorp, W. P. Three-Dimensional Transformations for Goal-Directed Action. *Annual Review of Neuroscience* **34**, 309–331 (2011).

5. Aagten-Murphy, D. & Bays, P. M. Independent working memory resources for egocentric and allocentric spatial information. *PLOS Computational Biology* **15**, e1006563 (2019).

6. Bharmauria, V., Sajad, A., Yan, X., Wang, H. & Crawford, J. D. Spatiotemporal Coding in the Macaque Supplementary Eye Fields: Landmark Influence in the Target-to-Gaze Transformation. *eNeuro* **8**, (2021).

7. Bharmauria, V. *et al.* Integration of eye-centered and landmark-centered codes in frontal eye field gaze responses. *Cerebral Cortex* **bhaa090**, https://doi.org/10.1093/cercor/bhaa090 (2020).

8. Chen, Y., Monaco, S. & Crawford, J. D. Neural substrates for allocentric-to-egocentric conversion of remembered reach targets in humans. *European Journal of Neuroscience* **47**, 901–917 (2018).

9. Byrne, P. A. & Crawford, J. D. Cue Reliability and a Landmark Stability Heuristic Determine Relative Weighting Between Egocentric and Allocentric Visual Information in Memory-Guided Reach. *Journal of Neurophysiology* **103**, 3054–3069 (2010).

10. Karimpur, H., Kurz, J. & Fiehler, K. The role of perception and action on the use of allocentric information in a large-scale virtual environment. *Experimental Brain Research* 1–14 (2020) doi:10.1007/s00221-020-05839-2.

11. Lew, T. F. & Vul, E. Ensemble clustering in visual working memory biases location memories and reduces the Weber noise of relative positions. *Journal of Vision* **15**, 10 (2015).

12. Mutluturk, A. & Boduroglu, A. Effects of spatial configurations on the resolution of spatial working memory. *Attention, Perception, & Psychophysics* **76**, 2276–2285 (2014).

13. Chen, Y. & Crawford, J. D. Allocentric representations for target memory and reaching in human cortex. *Annals of the New York Academy of Sciences* **1464**, 142–155 (2020).

14. Chen, Y. *et al.* Allocentric versus egocentric representation of remembered reach targets in human cortex. *The Journal of neuroscience : the official journal of the Society for Neuroscience* **34**, 12515–26 (2014).

15. Milner, D. & Goodale, M. *The Visual Brain in Action*. (Oxford University Press, 2006). doi:10.1093/acprof:oso/9780198524724.001.0001.

16. Schenk, T. No Dissociation between Perception and Action in Patient DF When Haptic Feedback is Withdrawn. *J. Neurosci.* **32**, 2013–2017 (2012).

17. Spillmann, L., Dresp-Langley, B. & Tseng, C. Beyond the classical receptive field: The effect of contextual stimuli. *Journal of Vision* **15**, 7–7 (2015).

18. Wurtz, R. H. Recounting the impact of Hubel and Wiesel. *J Physiol* **587**, 2817–2823 (2009).

19. Edelman, J. A. & Goldberg, M. E. Saccade-Related Activity in the Primate Superior Colliculus Depends on the Presence of Local Landmarks at the Saccade Endpoint. *Journal of Neurophysiology* **90**, 1728–1736 (2003).

20. Wilber, A. A., Clark, B. J., Forster, T. C., Tatsuno, M. & McNaughton, B. L. Interaction of egocentric and world-centered reference frames in the rat posterior parietal cortex. *Journal of Neuroscience* **34**, 5431–5446 (2014).

21. Snyder, L. H., Grieve, K. L., Brotchie, P. & Andersen, R. A. Separate body- and world-referenced representations of visual space in parietal cortex. *Nature* **394**, 887–891 (1998).

22. Uchimura, M; Kumano, H; Kitazawa, S. Rapid allocentric coding in the monkey precuneus. in *Society for Neuroscience* 589.24/ GG19 (2017).

23. DeSouza, J. F. X. *et al.* Intrinsic reference frames of superior colliculus visuomotor receptive fields during head-unrestrained gaze shifts. *The Journal of neuroscience : the official journal of the Society for Neuroscience* **31**, 18313–26 (2011).

24. Keith, G. P., DeSouza, J. F. X., Yan, X., Wang, H. & Crawford, J. D. A method for mapping response fields and determining intrinsic reference frames of single-unit activity: Applied to 3D head-unrestrained gaze shifts. *Journal of Neuroscience Methods* **180**, 171–184 (2009).

25. Sadeh, M., Sajad, A., Wang, H., Yan, X. & Crawford, J. D. Spatial transformations between superior colliculus visual and motor response fields during

head-unrestrained gaze shifts. *European Journal of Neuroscience* **42**, 2934–2951 (2015).

26. Sajad, A. *et al.* Visual-Motor Transformations Within Frontal Eye Fields During Head-Unrestrained Gaze Shifts in the Monkey. *Cerebral cortex (New York, N.Y. : 1991)* **25**, 3932–52 (2015).

27. Li, J. *et al.* Effect of allocentric landmarks on primate gaze behavior in a cue conflict task. *Journal of vision* **17**, 20 (2017).

28. Blohm, G., Khan, A. Z., Ren, L., Schreiber, K. M. & Crawford, J. D. Depth estimation from retinal disparity requires eye and head orientation signals. *Journal of Vision* **8**, 3–4 (2008).

29. Klier, E. M. & Crawford, J. D. Human oculomotor system accounts for 3-D eye orientation in the visual-motor transformation for saccades. *Journal of neurophysiology* **80**, 2274–94 (1998).

30. Crawford, J. D., Ceylan, M. Z., Klier, E. M. & Guitton, D. Three-Dimensional Eye-Head Coordination During Gaze Saccades in the Primate. *Journal of Neurophysiology* **81**, 1760–1782 (1999).

31. Duhamel, J.-R., Bremmer, F., BenHamed, S. & Graf, W. Spatial invariance of visual receptive fields in parietal cortex neurons. *Nature* **389**, 845–848 (1997).

32. Schlack, A., Sterbing-D'Angelo, S. J., Hartung, K., Hoffmann, K.-P. & Bremmer, F. Multisensory space representations in the macaque ventral intraparietal area. *J Neurosci* **25**, 4616–4625 (2005).

33. Purcell, B. A., Weigand, P. K. & Schall, J. D. Supplementary eye field during visual search: Salience, cognitive control, and performance monitoring. *Journal of Neuroscience* **32**, 10273–10285 (2012).

34. Sajad, A., Sadeh, M. & Crawford, J. D. *Spatiotemporal transformations for gaze control*. *Physiological reports* vol. 8 (NLM (Medline), 2020).

35. Olson, C. R. & Gettner, S. N. Object-centered direction selectivity in the macaque supplementary eye field. *Science (New York, N.Y.)* **269**, 985–8 (1995).

36. Tremblay, L., Gettner, S. N. & Olson, C. R. Neurons With Object-Centered Spatial Selectivity in Macaque SEF: Do They Represent Locations or Rules? *Journal of Neurophysiology* **87**, 333–350 (2002).

37. Fiehler, K., Wolf, C., Klinghammer, M. & Blohm, G. Integration of egocentric and allocentric information during memory-guided reaching to images of a natural environment. *Frontiers in Human Neuroscience* **8**, 636 (2014).

38. Klinghammer, M., Blohm, G. & Fiehler, K. Scene Configuration and Object Reliability Affect the Use of Allocentric Information for Memory-Guided Reaching. *Frontiers in Neuroscience* **11**, 204 (2017).

39. Blohm, G. & Crawford, J. D. Computations for geometrically accurate visually guided reaching in 3-D space. *Journal of vision* **7**, 4.1-22 (2007).

40. Khazali, M. F., Ramezanpour, H. & Their, P. V1 neurons encode the perceptual compensation of false torsion arising from Listing's law. *Proceedings of the National Academy of Sciences of the United States of America* **117**, 18799–18809 (2020).

41. van Polanen, V. & Davare, M. Interactions between dorsal and ventral streams for controlling skilled grasp. *Neuropsychologia* **79**, 186–191 (2015).

42. Milner, A. D. How do the two visual streams interact with each other? *Experimental Brain Research* vol. 235 1297–1308 (2017).

43. Budisavljevic, S. *et al.* Cross-talk connections underlying dorsal and ventral stream integration during hand actions. **103**, 224–239 (2018).

44. Pierce, J. E., Clementz, B. A. & McDowell, J. E. Saccades: Fundamentals and Neural Mechanisms. in 11–71 (Springer, Cham, 2019). doi:10.1007/978-3-030-20085-5_2.

45. O'Keefe, J. & Dostrovsky, J. The hippocampus as a spatial map. Preliminary evidence from unit activity in the freely-moving rat. *Brain Research* **34**, 171–175 (1971).

46. O'Keefe, J. Place units in the hippocampus of the freely moving rat. *Experimental Neurology* **51**, 78–109 (1976).

47. Froehler, M. T. & Duffy, C. J. Cortical neurons encoding path and place: Where you go is where you are. *Science* **295**, 2462–2465 (2002).

48. Haggerty, D. C. & Ji, D. Activities of visual cortical and hippocampal neurons co-fluctuate in freely moving rats during spatial behavior. *eLife* **4**, (2015).

49. Hindy, N. C., Avery, E. W. & Turk-Browne, N. B. Hippocampal-neocortical interactions sharpen over time for predictive actions. *Nature Communications* **10**, 1–13 (2019).

50. Saleem, A. B., Diamanti, E. M., Fournier, J., Harris, K. D. & Carandini, M. Coherent encoding of subjective spatial position in visual cortex and hippocampus. *Nature* **562**, 124–127 (2018).

51. Gazzaley, A. *et al.* Functional Interactions between Prefrontal and Visual Association Cortex Contribute to Top-Down Modulation of Visual Processing. doi:10.1093/cercor/bhm113.

52. Schall, J. D. Visuomotor Functions in the Frontal Lobe. *Annual Review of Vision Science* **1**, 469–498 (2015).

53. Munoz, D. P. Commentary: Saccadic eye movements: overview of neural circuitry. *Progress in Brain Research* **140**, 89–96 (2002).

54. Bruce, C. J. & Goldberg, M. E. Primate frontal eye fields. I. Single neurons discharging before saccades. *Journal of Neurophysiology* **53**, 603–635 (1985).

55. Klier, E. M., Wang, H. & Crawford, J. D. The superior colliculus encodes gaze commands in retinal coordinates. *Nature Neuroscience* **4**, 627–632 (2001).

56. Bremmer, F., Kaminiarz, A., Klingenhoefer, S. & Churan, J. Decoding Target Distance and Saccade Amplitude from Population Activity in the Macaque Lateral Intraparietal Area (LIP). *Frontiers in Integrative Neuroscience* **10**, 30 (2016).

57. Brandman, D. M., Cash, S. S. & Hochberg, L. R. Review: Human intracortical recording and neural decoding for brain computer interfaces. *IEEE transactions on neural systems and rehabilitation engineering : a publication of the IEEE Engineering in Medicine and Biology Society* **25**, 1687 (2017).

58. Bharmauria, V. *et al.* Network-selectivity and stimulus-discrimination in the primary visual cortex: cell-assembly dynamics. *European Journal of Neuroscience* **43**, 204–219 (2015).

59. Levy, M., Sporns, O. & MacLean, J. N. Network Analysis of Murine Cortical Dynamics Implicates Untuned Neurons in Visual Stimulus Coding. *Cell Reports* **31**, 107483 (2020).

60. Pruszynski, J. A. & Zylberberg, J. The language of the brain: real-world neural population codes. *Current Opinion in Neurobiology* **58**, 30–36 (2019).

61. Zylberberg, J. The role of untuned neurons in sensory information coding. *bioRxiv* 134379 (2018) doi:10.1101/134379.

62. Sajad, A., Sadeh, M., Yan, X., Wang, H. & Crawford, J. D. Transition from Target to Gaze Coding in Primate Frontal Eye Field during Memory Delay and Memory-Motor Transformation. *eNeuro* **3**, (2016).

Supplementary Figures and Analysis

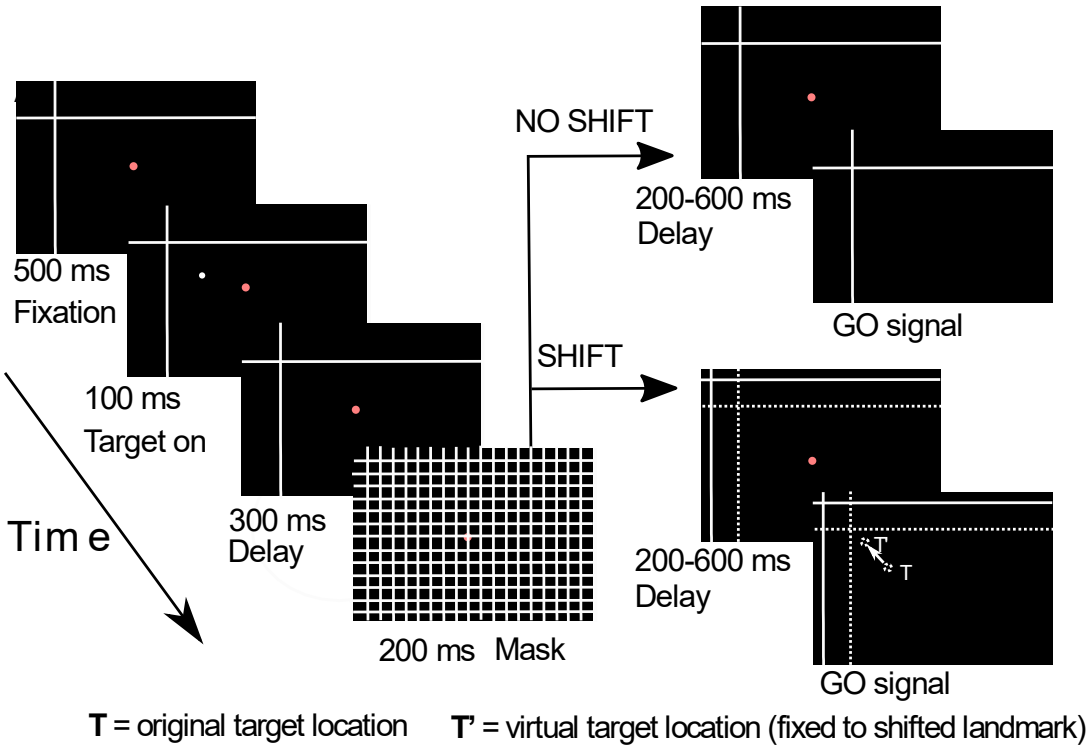

Figure i: Complete memory-delay / landmark paradigm, showing the initial landmark-target combinations analyzed here, and later cue-conflict and saccade 'go' signals that occurred later in the time course (not analyzed here). The monkey starts the trial by fixating a central red dot for 500 ms in the presence of two white intersecting lines (landmark). Then a white dot (target) is flashed (100 ms) in one of four possible locations relative to the landmark, followed by 300 ms delay (the first portion of this delay corresponds to the analysis period in this study) and a grid-like mask (200 ms). After mask offset the landmark either shifted in one of eight radial locations from the original location (or did not shift). Then after an additional delay period (200 – 600 ms) the fixation point was extinguished which served as a go signal for the animal to saccade to the remembered target location. Note that the latter event occurred well after the data described in the current study. The animal was rewarded for landing its gaze (G) within a circle of radius 8-12° around the original target. Gray box: Portion of the stimulus associated with the visual response.

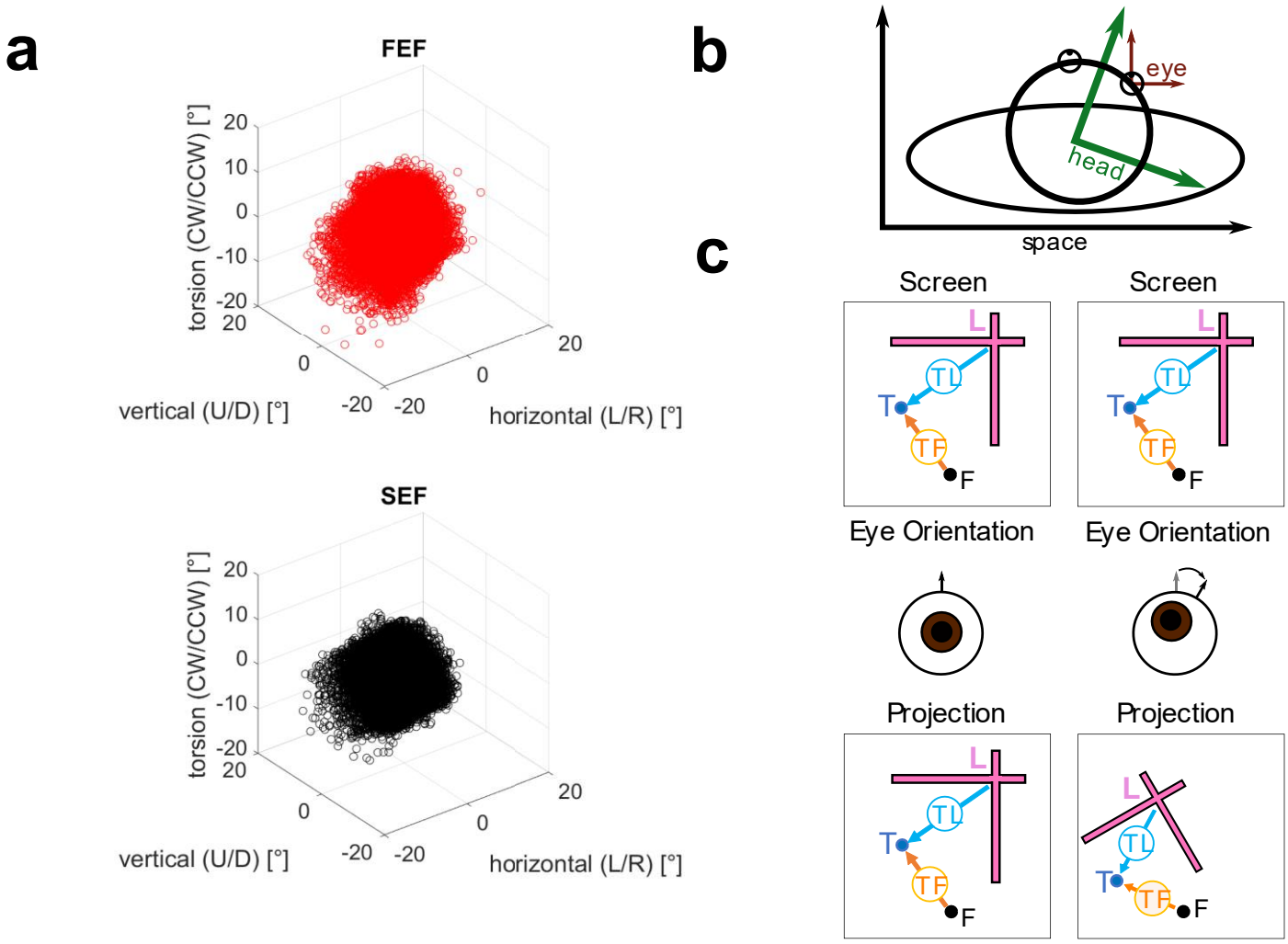

Figure ii: (a) Scatter plot of eye orientation at initial fixation position. Orientation is given by the composite of eye-in-head and head-in-space orientation. Data from every trial used in the analysis are shown. **(b)** Schematic of how different rotation in different coordinate systems interact with each other. As one can see a change in head-in-space orientation induces changes for the eye-in-space orientation. **(c)** Schematic of how eye orientation in space influence projection of the stimulus. The top row represents the screen, the middle row show a schematic eye orientation and the bottom row show the resulting projection based on this eye orientation. As one can see a tilted and rotated eye result in a rotated and compressed projection of the presented scene. Thus, leading to different projected TL vectors for the same TLC. The amount of compression is greatly exaggerated for demonstrative purposes.

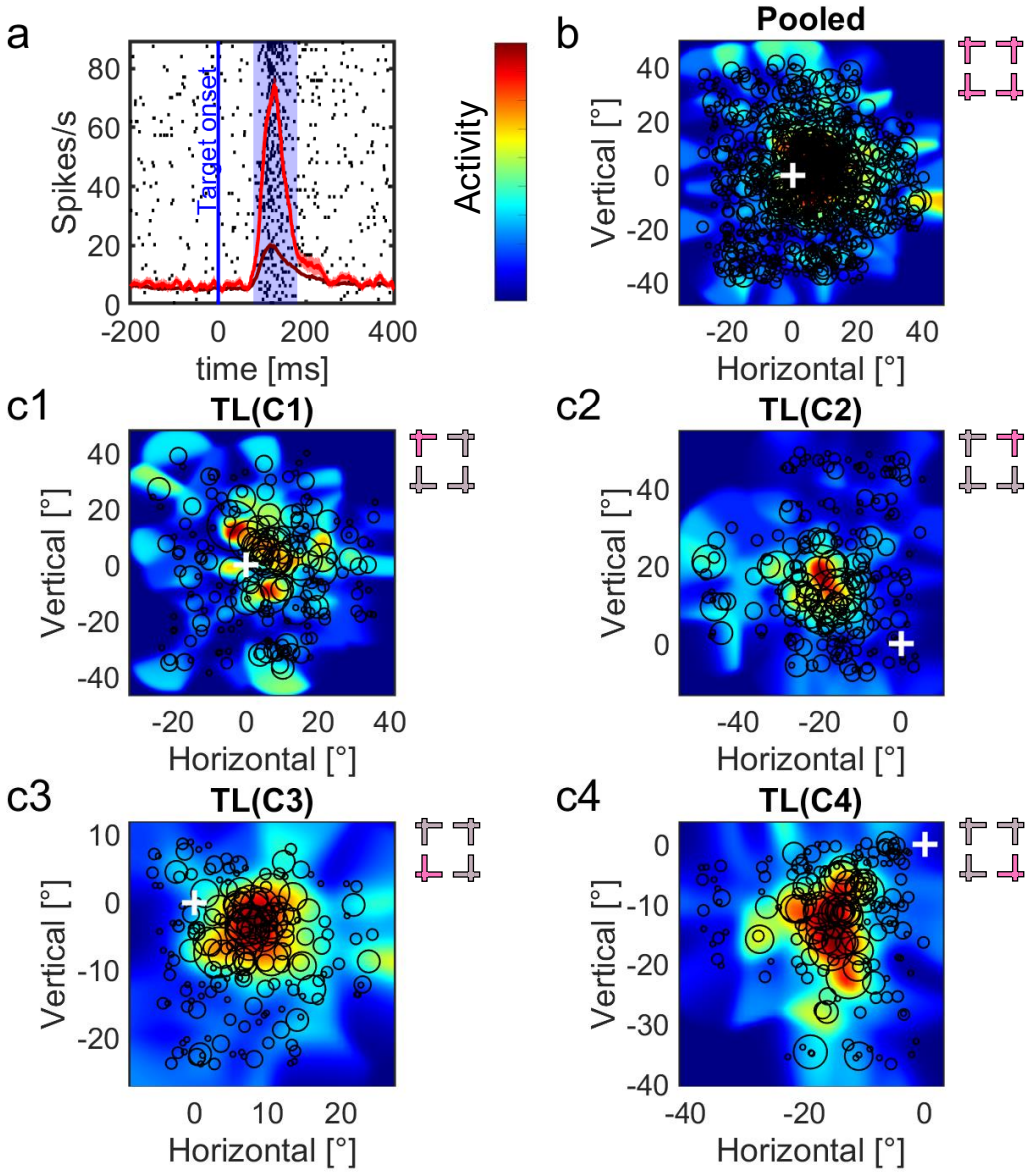

Figure iii: Typical example of a visual response analysis (for SEF neuron). (A) Shows the raster of the neuronal activity. The vertical blue line indicates the target onset and the

blue shaded area the time window used for further analysis. The faint red line shows the activity density for all trials, the red line the activity for the 10 % trials with the highest activity in the time window between 80 ms to 180 ms after target onset. (B) Shows the non-parametric fit of the neuron's response field. The color scale on the left indicates activation ranging from low (blue) to high (red). The black circles' position show the position of a trial in the feature space. The size of the circle the corresponding neuronal activation in this trial in the analysed time window. The white cross denotes (0,0)), i.e., xyz. (C) Shows the same analysis with the same figure convention as (B) but here the trials are splitted according to their respective target-landmark-configuration (TL(Cn))

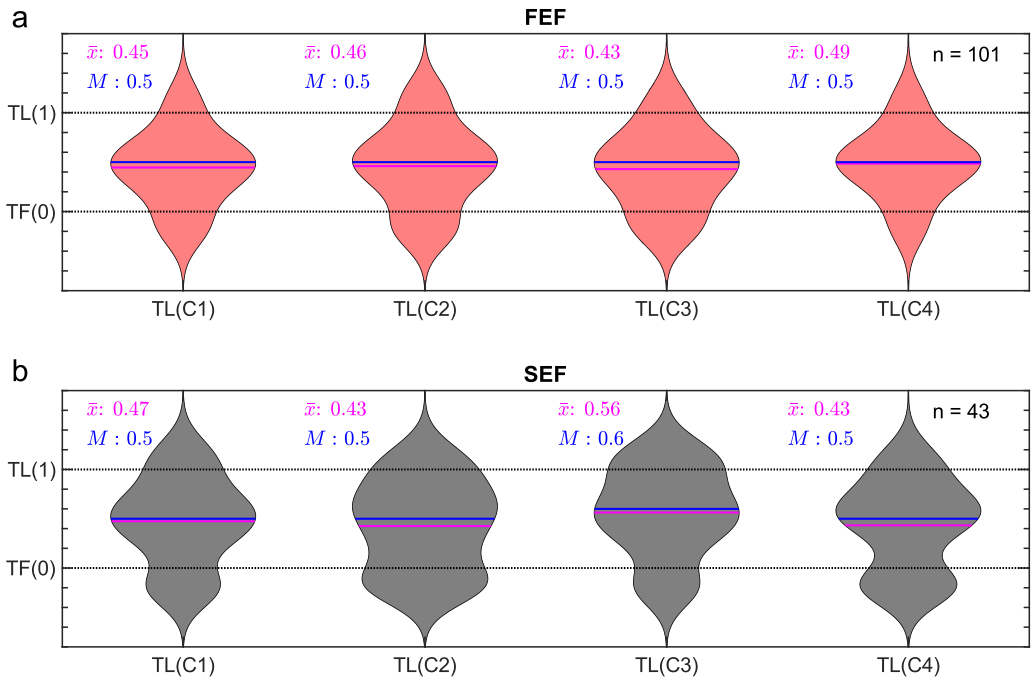

Figure iv: Violin plot of coding preference of neural population along the TF-TL continuum. The top row/red plots show data from FEF neurons. The lower row/black plots show data from SEF neurons. Blue lines represent the median, magenta lines represent the mean. (a) Best fit distribution for FEF neurons along the TF–TL continuum for each Target-Landmark configuration TLC1-4 (mean = 0.38, 0.36, 0.36, 0.41, median = 0.4, 0.4, 0.4, 0.4 respectively) (b) Best fit distribution for SEF neurons along the TF–TL continuum for for TLC1-4 (mean = 0.40, 0.44, 0.45, 0.32, median = 0.4, 0.4, 0.4, 0.4, respectively).

Figures

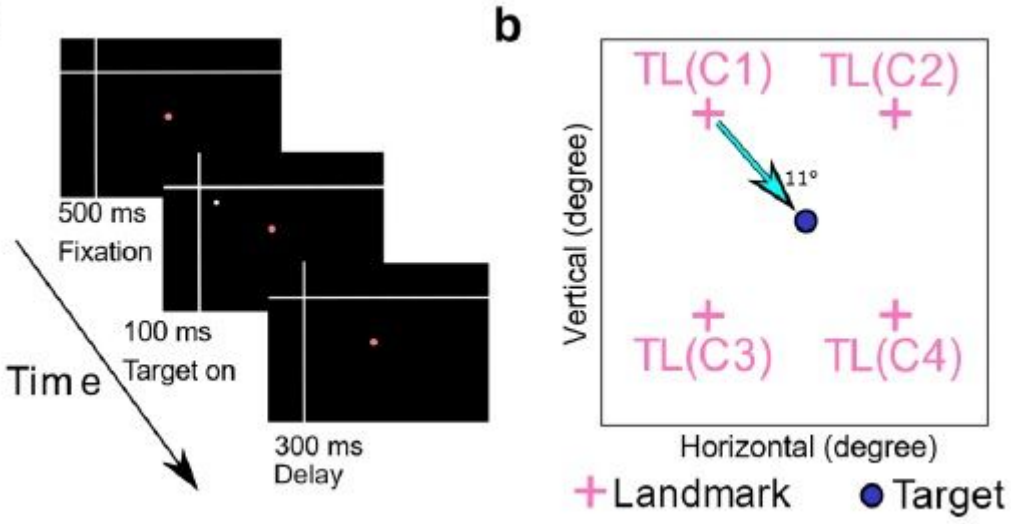

Figure 1

Experimental Paradigm (a) Initial stages of the memory-delay / landmark paradigm and its time course. The head unrestrained monkey starts the trial by fixating a central red dot for 500 ms in the presence of two white intersecting lines (landmark). Then a white dot (target) is flashed (100 ms) in one of four possible locations relative to the landmark, followed by a 300 ms delay. The remaining parts of the paradigm (not analyzed here) are presented in Supplementary Fig 1. (b) Schematic of the four possible target-landmark configurations (TLC1-4).

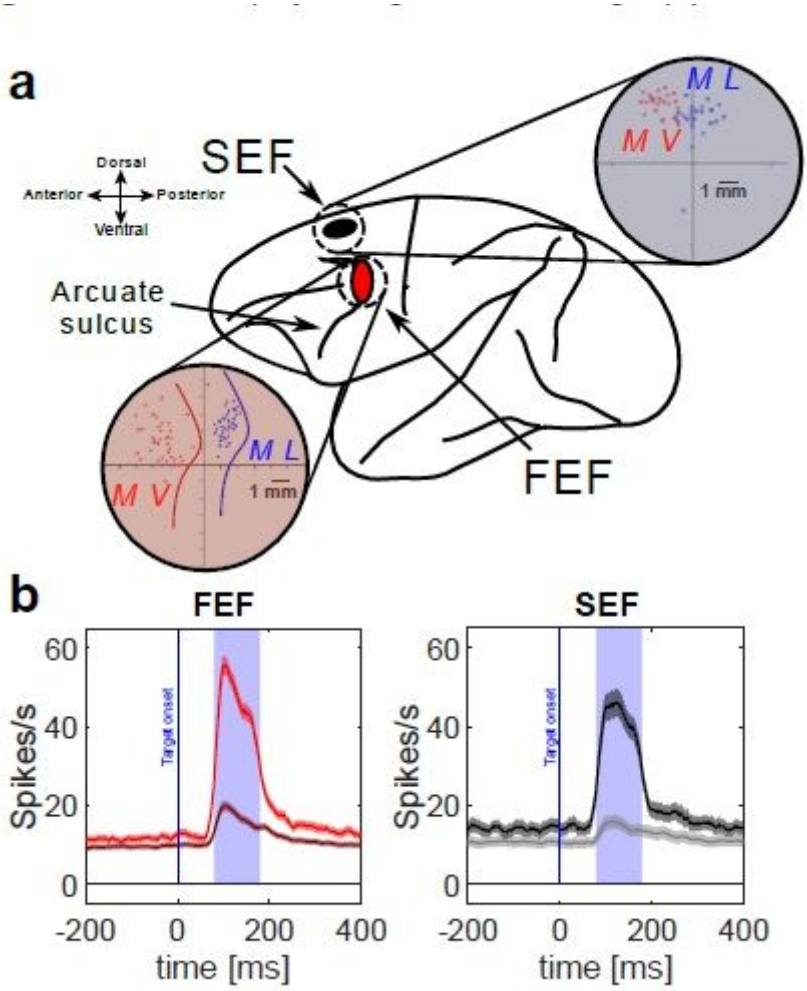

Figure 2

Electrophysiological recordings (a) The red ellipse represents the location of the FEF, the black ellipse represents the location of the SEF. The connected red and black disks represent the coordinates of our recording chambers, showing the sites (colored dots) of neural recordings for both monkeys (blue Monkey L, red Monkey V), also confirmed by microstimulation-evoked eye movements. Colored lines indicate the location of the arcuate sulcus within the recording chamber for both monkeys (b) Mean (± SD) of the spike-density plots of the visual responses for all FEF neurons (red) and SEF neurons (black/grey) analyzed in this study). The more robust plots (bright red/black) were derived from the top 10% responses for each neuron (corresponding to the 'hot' spot of the neuron's response field used to plot activity in most oculomotor studies), whereas the dark red / gray plots correspond to data from the entire sample (including the top 10%). The shaded areas show the temporal windows used for sampling data to quantify the visual response (ranging from 80ms to 180ms after target onset).

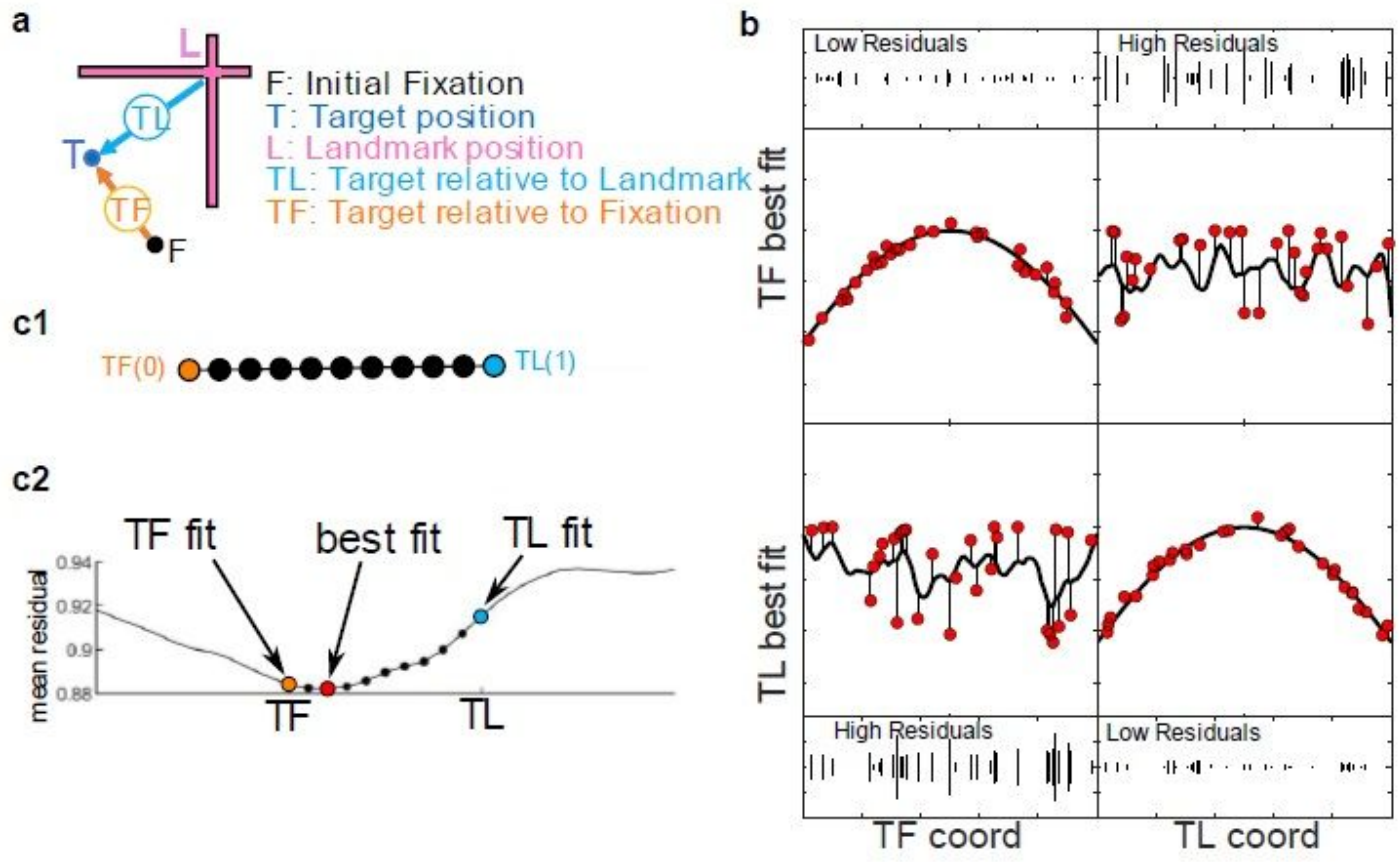

Figure 3

(a) Schematic for the spatial parameters of a single trial. The target position (TF) is shown in dark blue, the landmark position (L) is shown in magenta, the target position relative to the landmark (TL) is indicated by a cyan arrow, the initial fixation is indicated by the black dot and the target relative to initial gaze fixation (TF) is shown as an orange arrow. All positions were calculated in eye coordinates (b) Schematic of the logic behind the response field analysis. The x-axes represent the spatial coordinate. The y-axes show neural activity. Neural responses from individual trials are represented by the red dots. The black curving lines show the non-parametric fits which do not restrain the response field to a specific (e.g. gaussian) shape. The upper-left square shows activity from a neuronal response field that is tuned to TF coordinates and plotted relative to TL coordinates, resulting in a good fit with low residuals (difference between the fit and data, shown as vertical lines). The upper-right square shows activity from a neuronal response field tuned to TF coordinates but plotted in TL coordinates, resulting in a poor fit. Conversely, TF coordinates will provide poor fit, and TL coordinates will provide a good fit to a neuron tuned to TL coordinates (bottom panels). (c): Fitting data to intermediate TL-TF coordinates. (c1) Black circles show intermediate steps along the mathematical continuum between TF (represented as 0) and TL (represented at 1.0) Exemplary TF (orange) to TL (cyan). The red spot represents the best fit in the following example. (c2) Lower row: mean residuals for fits along the TF-TL continuum, including purely TF (orange), optimal (red), and TL (cyan) fits.

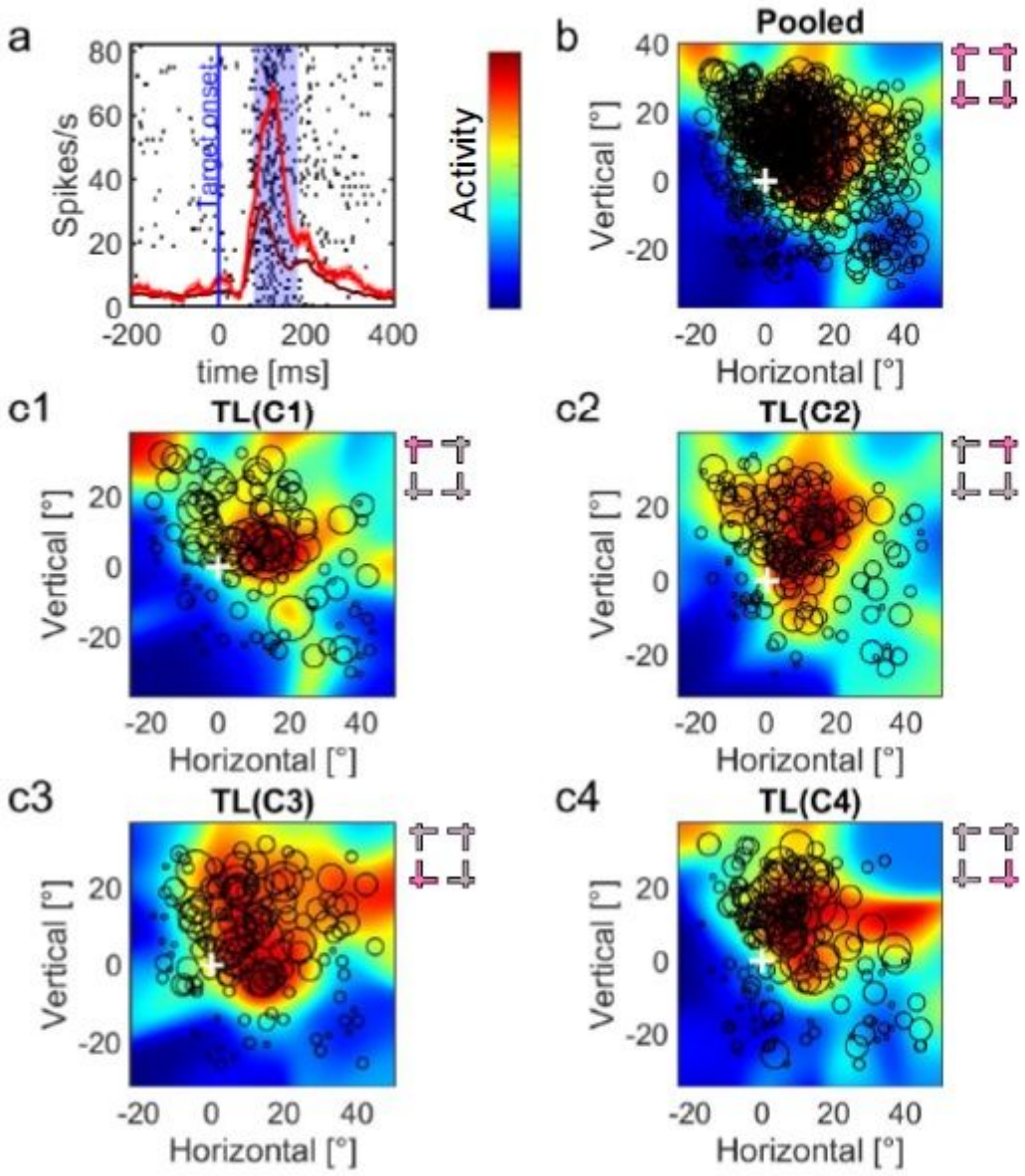

Figure 4

Typical example of a visual response field analysis (in this case for an FEF neuron). (a) Raster and spi e densit plot of the neuron's activit . The blue vertical line indicates the target onset and the blue shaded area the time window (80ms to 180 ms after target onset) used to quantify the visual response to the target. The dark red line shows the spike density for all trials (including the top 10%), the bright red line the activity for the 10 % trials with the highest activity in the analysis window. The confidence intervals show the standard error. (b) Shows the non-parametric fit of the neuron's response field, pooling data across all four landmark configurations (indicated by magenta crosses). The color scale on the left indicates the fit to activation ranging from low (blue) to high (red). The black circles indicate responses from individual trials, placed at the target stimulus's location and the diameter scaled to the response in the sampling window. The white crosses indicate the 0,0 point (fovea) in this coordinate system. (c1-c4)

Shows a similar analysis but computed separately for each landmark configuration (TLC1-4, indicated in magenta). cti ity

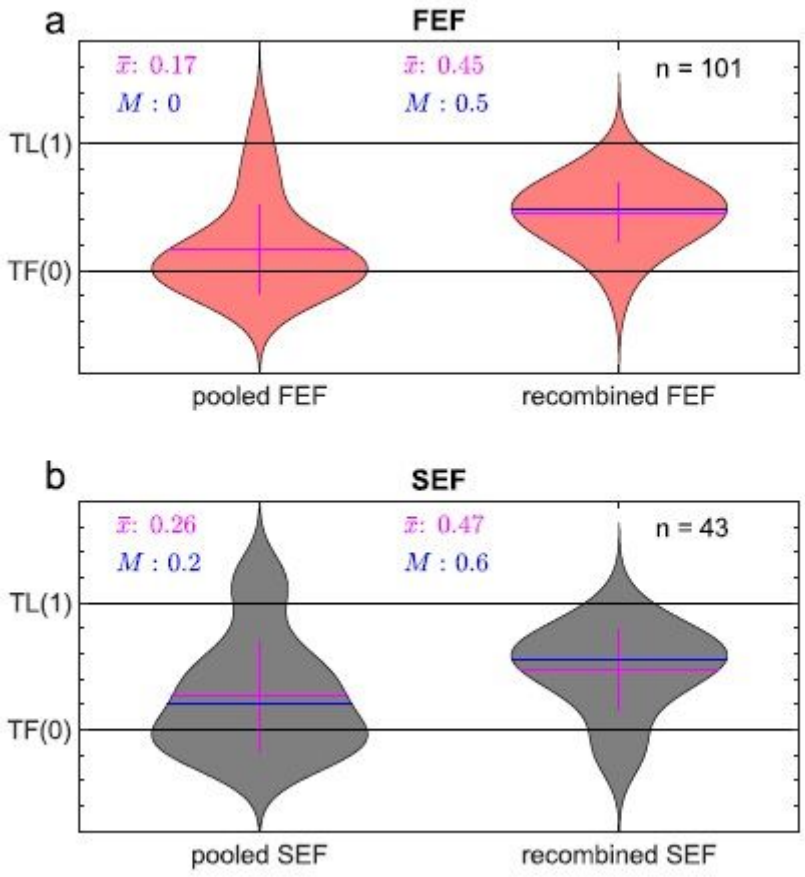

Figure 5

Violin plots of the distributions of best fits along the TF-TL continuum for all spatially tuned FEF neurons (a) and SEF neurons (b). The left side plots show fits made to the pooled data (across all four landmarks) for each neuron; the right-side plots show fits derived separately for each landmark configuration, then recombined by averaging the TF-TL score for each neuron. Blue lines represent the median; magenta lines represent the mean. FEF neurons (a) showed no significant deviation from TF(0) (mean = 0.17, median = 0) in the pooled analysis whereas the separate / recombined distributions (mean = 0.45, median 0.5) were significantly shifted toward TL(1). Likewise, SEF neurons (b) showed no significant shift from TF (mean = 0.26, median = 0.2), whereas the separate / recombined distributions (mean = 0.47, median = 0.6) were significantly shifted toward TL. See text for statistical details.

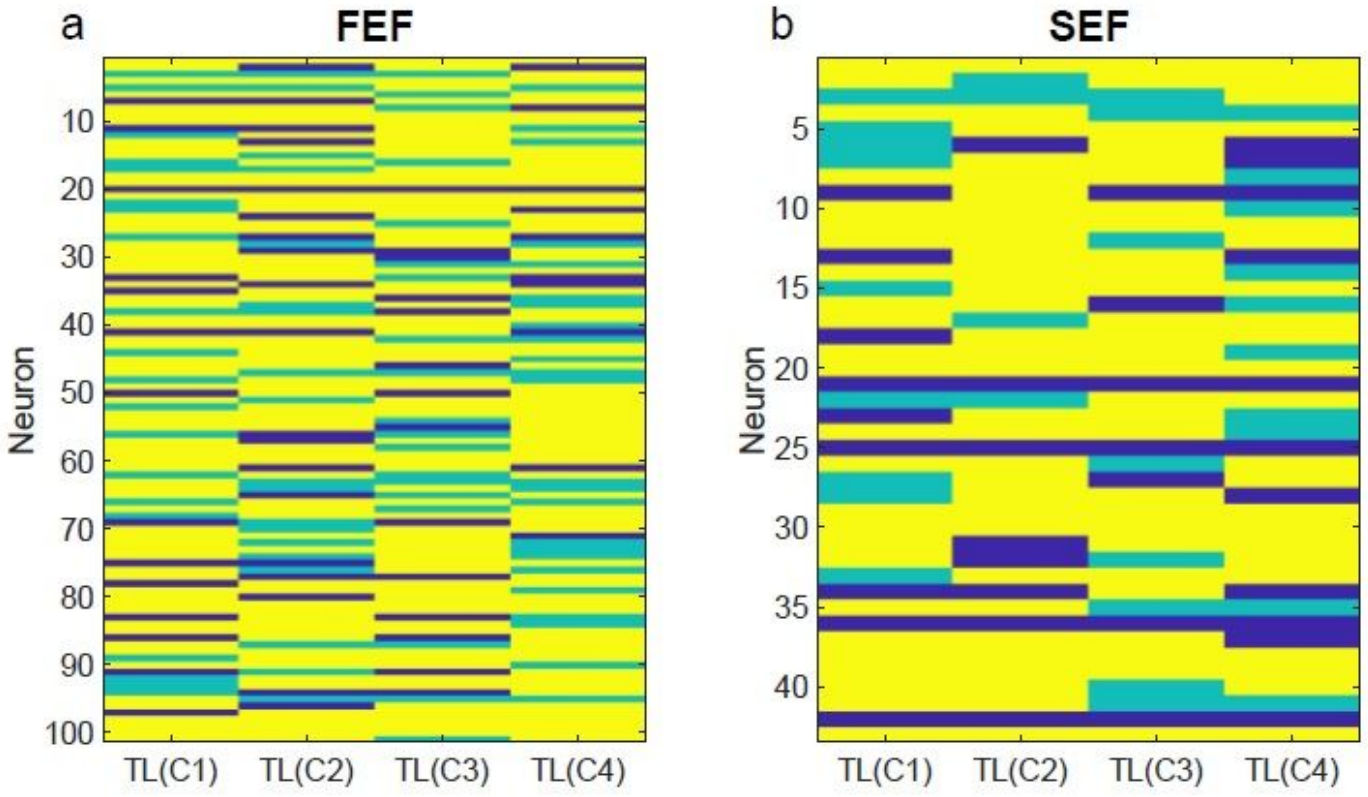

Figure 6

Neuron-by-neuron significance test for TF-TL shift, broken down by Landmark configuration (TLC 1-4). Left: FEF neurons Rigt: SEF neurons. The y axis identifies the neuron, the x axis the represents the TLC. Yellow cells are significantly different. From their respective randomized baseline describes in methods. Cyan cells are not significantly different. Blue cells are untuned neurons.